ARTICLE

doi:10.1038/nature13556

Non-cell-autonomous driving of tumour growth supports sub-clonal heterogeneity

Andriy Marusyk[1,2,3], Doris P. Tabassum[1,4], Philipp M. Altrock[5,6,7], Vanessa Almendro[1,2,3], Franziska Michor[5,6] & Kornelia Polyak[1,2,3,4,8]

Cancers arise through a process of somatic evolution that can result in substantial sub-clonal heterogeneity within tumours. The mechanisms responsible for the coexistence of distinct sub-clones and the biological consequences of this coexistence remain poorly understood. Here we used a mouse xenograft model to investigate the impact of sub-clonal heterogeneity on tumour phenotypes and the competitive expansion of individual clones. We found that tumour growth can be driven by a minor cell subpopulation, which enhances the proliferation of all cells within a tumour by overcoming environmental constraints and yet can be outcompeted by faster proliferating competitors, resulting in tumour collapse. We developed a mathematical modelling framework to identify the rules underlying the generation of intra-tumour clonal heterogeneity. We found that non-cell-autonomous driving of tumour growth, together with clonal interference, stabilizes sub-clonal heterogeneity, thereby enabling inter-clonal interactions that can lead to new phenotypic traits.

Cancers result from genetic and epigenetic changes that fuel Darwinian somatic evolution[1,2]. Until recently, the evolution was assumed to proceed as a linear succession of clonal expansions triggered by acquisition of strong driver mutations that progressively increase cell fitness and lead to selective sweeps[3]. However, recent data from tumour genome sequencing studies and single-cell based analyses has revealed substantial genetic heterogeneity within tumours, including sub-clonal differences in driver mutations[4–8]. This contradicts the linear succession model and challenges the assumption of tumour evolution being driven by mutations providing strong clone-specific selective advantages. Furthermore, clonal heterogeneity raises the possibility of biologically and clinically important interactions between distinct clones[9,10].

Many oncogenic mutations confer a cell-autonomous fitness advantage by either providing independence from growth factors or abolishing an apoptotic response. These mutations are thus expected to drive clonal expansions[11]. At the same time, tumour progression is frequently limited by microenvironmental constraints[12–14] that cannot be overcome by a cell-autonomous increase in proliferation rates. Instead, progression depends on alterations of the microenvironment, mediated by factors acting non-cell-autonomously, such as metalloproteinases and cytokines. It is unclear whether these secreted factors preferentially benefit the 'producer' clone(s) enabling their clonal dominance.

A model of clonal heterogeneity

Understanding clonal heterogeneity has been hindered by the lack of suitable experimental models. Although patient tumour-derived xenograft studies using clonal tracing can be insightful, their utility is limited by the challenges in deciphering mechanisms that underlie biological differences between sub-clones. We aimed to bypass these challenges by experimentally defining sub-populations via overexpression of factors previously implicated in tumour progression. We decided to exploit a scenario of a tumour that is 'stuck' in a microenvironmentally constrained progression bottleneck, which is relevant for clinically asymptomatic cancers, dormant micro-metastatic lesions and perhaps early clinically undetectable stages of tumour development. This scenario offers two key advantages. First, in contrast to a rapidly growing tumour, the constrained population size of non-growing tumours composed of rapidly cycling cells is expected to intensify competition for limited microenvironmental resources. This enhances the detection of differences in competitive fitness. Second, the indolent morphology and lack of net tumour growth should facilitate the detection of increase in tumour growth and metastasis.

In search of tumours satisfying these criteria, we analysed a panel of breast cancer-derived cell lines for tumours formed by orthotopic transplantation into the mammary fat pads of immunodeficient *Foxn1*^{nu} (nu) mice. Whereas most of the tested cell lines either failed to produce tumours or formed tumours that grew too rapidly (for example, SUM149PT cells), the MDA-MB-468 cell line formed indolent tumours which, upon reaching 2–5 mm in diameter, showed very slow growth rates (Fig. 1a and data not shown). Despite slow net growth, the tumour cells were actively proliferating: 80–90% of them were in the cell cycle based on Ki-67 staining, and 20–30% were in S phase based on 5-bromodeoxyuridine (BrdU) incorporation (Fig. 1b). The slow net tumour growth indicated that cell proliferation was counterbalanced by cell death. Indeed, 1–3% of the cells were apoptotic. Tumours contained large necrotic areas indicating substantial necrotic cell death (Fig. 1b).

We used MDA-MB-468 cells to generate a panel of sub-lines (henceforth called 'sub-clones') defined by the lentiviral overexpression of a single secreted factor. Each factor had been previously implicated in tumour progression, along with reported high expression in breast carcinoma cells of patients (Fig. 1c and Extended Data Table 1). Given the recently reported variability in clonal proliferation dynamics[15] and to minimize the confounding influences of genetic/epigenetic heterogeneity within the cell lines, we used pools of transduced cells rather than single cell-derived clones. This panel enabled us to compare phenotypic properties of tumours and clonal expansions under two circumstances: (1) each sub-clone competing against parental cells (monoclonal tumours), and (2) sub-clones competing against all other sub-clones (polyclonal tumours)

[1]Department of Medical Oncology, Dana-Farber Cancer Institute, Boston, Massachusetts 02215, USA. [2]Department of Medicine, Brigham and Women's Hospital, Boston, Massachusetts 02115, USA. [3]Department of Medicine, Harvard Medical School, Boston, Massachusetts 02115, USA. [4]BBS Program, Harvard Medical School, Boston, Massachusetts 02115, USA. [5]Department of Biostatistics and Computational Biology, Dana-Farber Cancer Institute, Boston, Massachusetts 02215, USA. [6]Department of Biostatistics, Harvard School of Public Health, Boston, Massachusetts 02115, USA. [7]Program for Evolutionary Dynamics, Harvard University, Cambridge, Massachusetts 02138, USA. [8]Harvard Stem Cell Institute and the Broad Institute, Cambridge, Massachusetts 02138, USA.

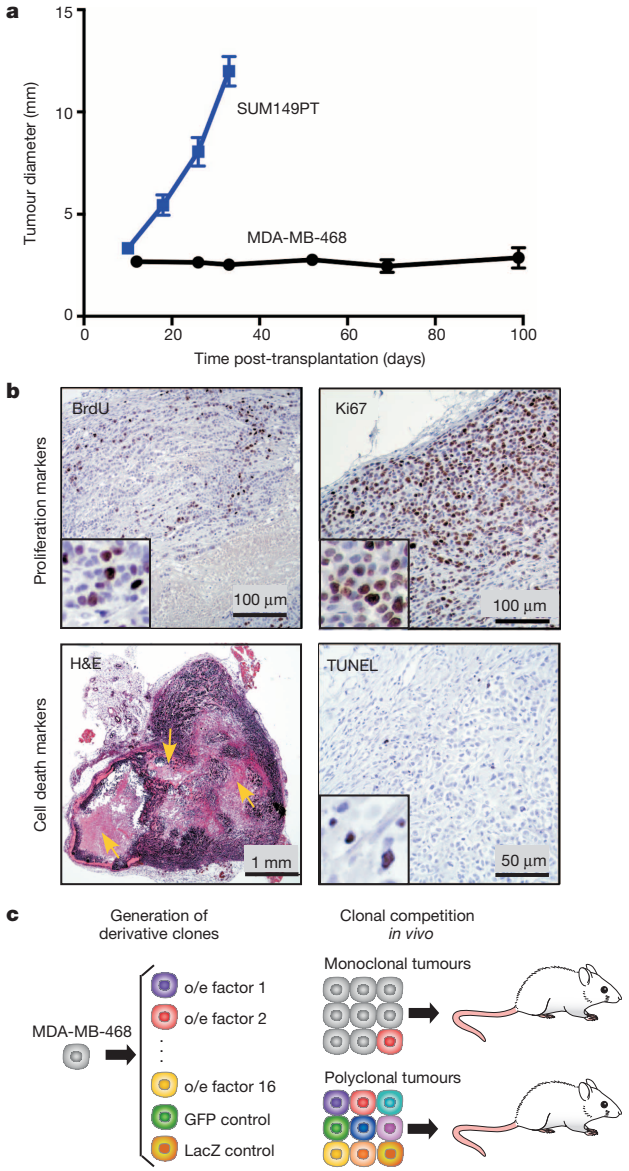

Figure 1 | Experimental system. **a**, Growth of tumours upon mammary fat pad transplantation of indicated cell lines, $n = 10$ per group, combined data from 2 independent experiments, error bars indicate s.e.m. **b**, Representative images of indicated staining. Arrows indicate necrotic areas. H&E, haematoxylin and eosin. **c**, Experimental scheme.

(Fig. 1c). We had 18 sub-clones in total. In order to maintain equal initial clonal proportions in all tumours, we employed the cell number ratio of 1:18 between a sub-clone and parental competitors.

Non-cell-autonomous tumour driving

We first investigated whether individual sub-clones, initially present as a minor sub-population competing against parental cells, could affect tumour properties. We focused on tumour growth and metastasis, features that are most relevant clinically and amenable to quantification. Although we observed variability between the groups in morphology, proliferation and vascularization (Extended Data Fig. 1), only the chemokine (C-C motif) ligand 5 (CCL5) and interleukin 11 (IL11) overexpressing sub-clones were able to enhance tumour growth (Fig. 2a, b). None of the tumours were metastatic, as evaluated by *in vivo* bioluminescence imaging and examination of draining lymph nodes, peritoneal walls and bone marrow (data not shown).

We then analysed the population frequencies of individual sub-clones within the tumours using a genomic quantitative polymerase chain reaction (qPCR) approach, using clone-specific and reference amplicons (Extended Data Fig. 2). Surprisingly, we observed no strict correlation between the increase in sub-clonal frequencies and the growth rate of tumours (Fig. 2a–c). The LOXL3-overexpressing sub-clone underwent the greatest (~tenfold) expansion in population frequency, yet failed to promote overall tumour growth. On the other hand, both CCL5 and IL11, each capable of driving outgrowth of tumours, exhibited approximately eightfold and fourfold expansion, respectively. To address the link between clone-specific expansion and tumour growth more directly, we calculated rates of expansion in cell numbers over the initially transplanted cells using a volume-based cellularity inference of 4.1×10^5 cells per mm^3 (Fig. 2d, Extended Data Fig. 3a). Only IL11 was capable of non-cell-autonomous tumour growth driving. We saw enhanced expansion of both IL11-expressing and parental cells. Increased growth of CCL5-driven tumours was only attributable to cell-autonomous expansion of CCL5-expressing cells. This finding was consistent with the observed delay in tumour outgrowth driven by CCL5 compared to IL11-driven tumours (Fig. 2a, inset).

We did not observe a positive correlation between tumour weights and final percentages of IL11 expressing cells (Extended Data Fig. 4a). An increase in the initial frequency of the IL11 sub-clone also did not further enhance tumour growth (Extended Data Fig. 4b). Parental cells expressed undetectable basal levels of IL11 (Extended Data Fig. 4c, d) and the non-cell-autonomous driving of tumour growth was observed with four independent derivations of the IL11 overexpressing sub-clones using two distinct lentiviral backbones that provide different levels of expression (Extended Data Fig. 4c–e). This observation strongly suggests that the phenomenon was IL11-specific and did not require additional stochastic events.

We then initiated tumours in which all the sub-clones, present at the initial 1:18 ratio, were set to compete against one another. These tumours grew faster than monoclonal tumours, suggesting additive growth-promoting interactions among the sub-clones (Fig. 2a). However, omitting the IL11 sub-clone (2:18 ratio of control LacZ sub-clone was used to maintain 1:18 ratio of the remaining sub-clones) blocked the increased growth of polyclonal tumours, reducing clonal expansions (Fig. 2e and Extended Data Fig. 5a). Therefore, non-cell-autonomous stimulation by IL11 was both necessary and sufficient to drive tumour growth.

Sub-clonal cooperation in metastasis

In addition to accelerated growth rates, polyclonal tumours displayed regions of extensive haemorrhage and multiple cysts (Fig. 2f), indicative of increased blood and lymphatic vessel leakage. Consistently, a large fraction of polyclonal tumours were metastatic: 7/12 analysed animals displayed lymph node metastases, 6/12 displayed metastatic nodes on the peritoneal wall and 4/7 contained tumour cells in the bone marrow (Fig. 2g). Animals bearing polyclonal tumours accumulated peritoneal fluid and demonstrated signs of systemic toxicity, requiring euthanasia at earlier time points compared to other groups.

FIGF was the only other sub-clone displaying elevated vascular leakage in monoclonal tumours, albeit with incomplete penetrance. Hence we asked whether the combination of IL11 and FIGF could recapitulate the metastatic phenotypes of polyclonal tumours. Indeed, FIGF/IL11 tumours displayed an increase in tumour volume and extensive haemorrhage (Fig. 2f, Extended Data Fig. 5b), with 4/4 animals presenting both lymph node and peritoneal wall metastases. Therefore, our data suggest that biological interactions between distinct sub-populations can lead to the emergence of new tumour phenotypes.

Mechanisms of IL11-driven tumour growth

Elevated tumour growth implies an increase in net cell proliferation rates, either by stimulating proliferation or by inhibiting cell death. IL11-driven tumours displayed a subtle, but significant, increase in proliferation rates compared to parental tumours (Fig. 3a). Apoptosis rates were similar (Extended Data Fig. 1b). This increase in cellular proliferation could result either from a direct autocrine/paracrine stimulation of cell

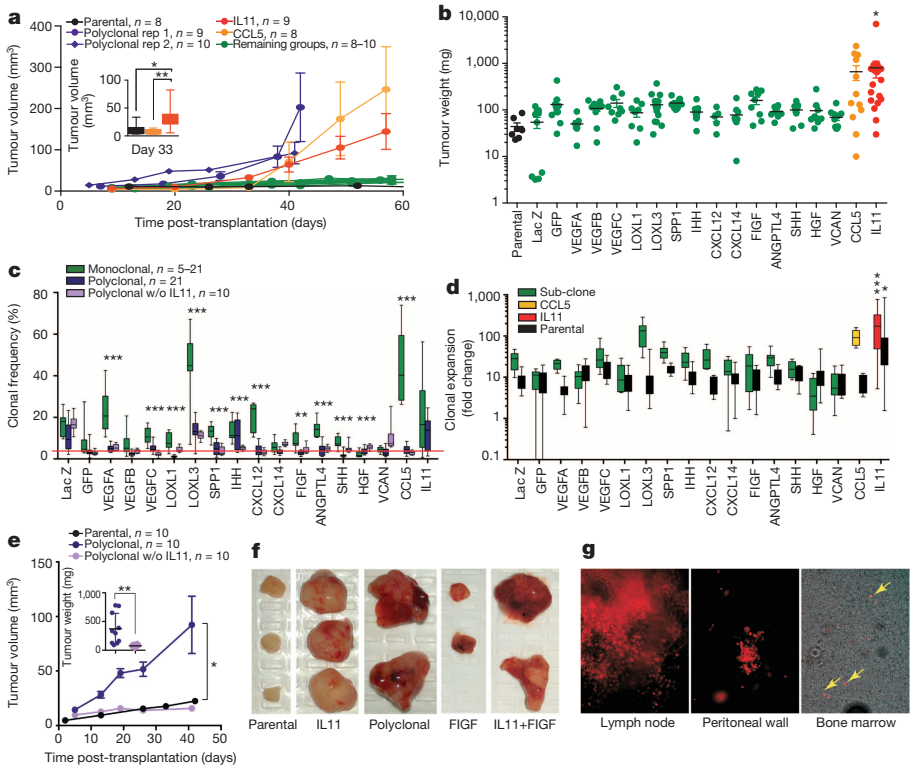

Figure 2 | Polyclonality affects tumour phenotypes. **a**, Tumour growth kinetics. **b**, Tumour weights. **c**, Sub-clones frequencies within tumours. Red line indicates initial frequency. **d**, Expansion (fold-change over initial cell number) of sub-clones and parental cells from monoclonal tumours shown in **c**. **e**, Tumour growth kinetics and weights (inset). **f**, Representative images of tumours. **g**, live fluorescent microscopy images of tumour cells (mCherry^{+}) in tissues. $*P < 0.05$, $**P < 0.01$ and $***P < 0.001$, respectively, of Student's *t*-test (**a**, **c**, **e**) or ANOVA multiple group comparison against parental (**b**) or LacZ (**d**) with Dunnett's correction. Error bars indicate s.e.m. Data shown are representative of at least 2 independent experiments.

growth or from indirect effects mediated by the microenvironment. IL11 signals through a unique and specific receptor, IL11Rα, that forms a signalling complex with the GP130 co-receptor shared with other IL6 cytokine family members[17]. IL11 promotes growth of gastric carcinoma via direct stimulation of epithelial cells[18,19]. Similar stimulation of tumour growth via non-cell-autonomous signalling between tumour cells, involving two related cytokines, IL6 and LIF, was reported in glioblastomas[20]. We therefore asked whether modulation of IL11Rα expression in carcinoma cells affects the ability of IL11 to induce tumour growth. Neither overexpression nor short hairpin (shRNA)-mediated downregulation of IL11Rα affected IL11-driven tumour growth (Fig. 3b and Extended Data Fig. 7). Furthermore, IL11 significantly promoted growth of 2/4 additional breast cancer cell lines despite low or undetectable levels of IL11Rα (Fig. 3c, d).

Independence of tumour growth from direct stimulation of tumour cells by IL11 prompted us to investigate changes in the tumour microenvironment. IL11-driven tumours displayed higher intratumoral vascular density compared to parental ones (Fig. 3e, f), more dispersed patterns of collagen organization and had more stromal fibroblasts (Extended Data Fig. 8). Both increased vascularization and reorganization of the extracellular matrix have been implicated in the promotion of tumour growth[21,22], suggesting that the tumour-promoting effects of IL11 may be attributable to microenvironmental changes.

Clonal competition dynamics

Contexts of polyclonal tumours strongly inhibited the expansion of individual sub-clones in comparison to monoclonal tumours (Fig. 2c). This phenomenon is known as clonal interference: when multiple clones with higher than average fitness emerge in a population at the same time, they interfere with each other; this slows down the rate of clonal evolution[16]. However, the reduced expansion of individual sub-clones in IL11-driven polyclonal tumours could also be the result of a growing population. Therefore, to distinguish between the effects of clonal interference and expanding tumour volume, we determined clonal expansions in slower growing polyclonal tumours without IL11 (Fig. 2c). We found that while the removal of IL11 significantly affected clonal composition of the tumours ($P < 0.0001$ for the interaction factor in a two-way ANOVA), expansion of most of the sub-clones remained inhibited. This indicates that clonal interference is a major determinant of the differences in the competitive dynamics in polyclonal tumours.

To investigate the rules of tumour growth and to predict clonal dynamics on a longer timescale, we then developed a mathematical framework incorporating clonal interference and heterogeneity. First, we investigated the growth behaviour of monoclonal tumours, finding that tumours exhibited an exponential growth pattern (Extended Data Fig. 3b). We then estimated the clone-specific exponential growth rates for each monoclonal growth experiment. With these rates we predicted tumour sizes in polyclonal tumours adding a dynamic interaction term (Fig. 4a, Extended Data Fig. 3c, d and Supplementary Information).

In order to account for interactions between a driver clone and other clones, we investigated a hierarchy of nested, increasingly complex mathematical descriptions of clonal dynamics for their ability to predict data from individual polyclonal growth experiments. The null hypothesis of no clonal interactions was easily rejected. The best agreement between model predictions and experimental observations in polyclonal tumours was achieved by including a constant positive growth effect of the IL11 clone on all other clones. Higher-order interactions involving multiple drivers did not improve the predictive power of the model. The best-fitting model was then used to predict heterogeneity in polyclonal tumours over longer timescales. In the absence of IL11, clonal heterogeneity was predicted to eventually vanish, as clones with the highest proliferation rates outcompete less fit clones. In contrast, non-cell-autonomous stimulation of cell growth supports clonal diversity over clinically relevant timescales (Fig. 4b).

As anti-cancer therapy exerts selective pressures that can affect evolutionary dynamics, we investigated the effect of treatment with doxorubicin, a commonly used chemotherapeutic agent in breast cancer, on the diversity of the tumour cell population. Two rounds of doxorubicin administration substantially inhibited tumour growth and cell proliferation in polyclonal tumours (Extended Data Fig. 6a, b). Instead of the expected changes in the expansion of specific sub-clones differing in drug sensitivity, we found that the amplitude of clonal expansion and

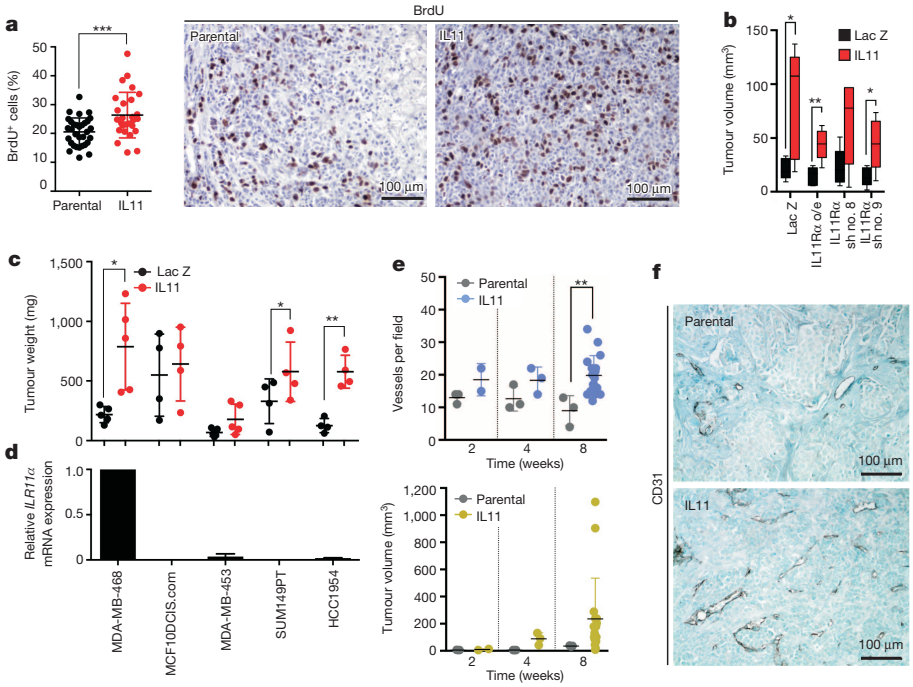

Figure 3 | IL11 drives tumour cell proliferation via microenvironmental changes. **a**, Quantification and representative images of anti-BrdU immunohistochemical staining in control and IL11-driven tumours. **b**, Tumour volumes 31 days post-transplantation of parental MDA-MB-468 cells, cells overexpressing or with downregulated IL11Rα, $n = 5$ per group **c**, Tumour weights of contralateral parental and IL11 expressing tumours formed by the indicated cell lines. **d**, Levels of expression of *IL11Rα* mRNA in indicated cell lines, normalized to MDA-MB-468. **e**, Quantification of average number of $CD31^+$ vessels per field and tumour volumes. **f**, Representative images of anti-CD31 immunohistochemical staining. $*P < 0.05$, $**P < 0.01$ and $***P < 0.001$, respectively of unpaired (**a**, **b**, **e**) or paired (**c**) Student's *t*-test. Error bars indicate s.e.m. Data shown are representative of at least 2 independent experiments.

contractions was increased compared to untreated tumours, reducing clonal diversity (Extended Data Fig. 6c, d). Therefore, even in the absence of selection for resistant subpopulations, doxorubicin treatment non-specifically amplified the effects of differences in competitive fitness. This observation was most probably a result of increased competition due to treatment-induced stabilization of the population size.

The lack of correlation between clonal expansion and tumour growth prompted examination of the competition between IL11 and LOXL3 sub-clones. The latter showed the strongest expansion in population frequency without being able to drive tumour growth (Fig. 2d). IL11 accelerated the growth of tumours with LOXL3 competitors beyond the growth rates seen with IL11/parental (IL11/P) controls (Fig. 4c),

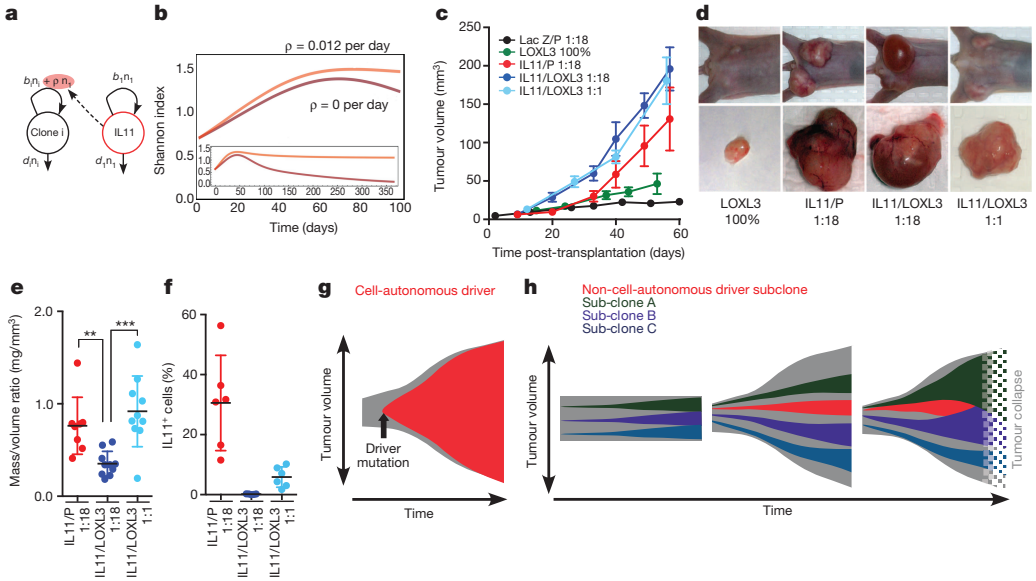

Figure 4 | Effect of IL11 on clonal dynamics. **a**, Outline of the linear model that best explains polyclonal dynamics (see Supplementary Information). **b**, Prediction of diversity over time without (dark) or with (light) non-cell-autonomous driver. **c**, Tumour growth kinetics, $n = 10$ per group. **d**, Representative images. **e**, Mass/volume ratios of tumours in **c**–**e** excluding cyst fluid, each dot represents an individual tumour, $**P < 0.01$, $***P < 0.001$; error bars indicate s.e.m. **f**, Final population frequencies of $IL11^+$ cells in the indicated tumours. **g**, **h**, Models of cell-autonomous (**g**) and non-cell-autonomous (**h**) driving of tumour growth. Data shown are representative of at least 2 independent experiments.

consistent with the ability of faster proliferating LOXL3 cells to obtain additional benefit from IL11. However, upon sample collection, 1:18 IL11/LOXL3 tumours contained very little solid tissue. Most of the volume was filled with interstitial fluid, probably a remnant of necrotic liquefaction, whereas 1:18 IL11/P and 1:1 IL11/LOXL3 tumours remained solid (Fig. 4d, e).

Analysis of clonal composition revealed that LOXL3 had outcompeted the IL11 sub-clone below the detectability threshold in 1:18 IL11/LOXL3 tumours. In contrast, 1:1 IL11/LOXL3 tumours contained reduced, but substantial proportions of IL11 cells (Fig. 4f). Loss of IL11 cells most probably reflects differences in proliferation rates rather than apoptotic elimination of slower dividing cells seen in other experimental contexts[23]. We did not observe elevated rates of apoptosis in IL11 cells bordering $LOXL3^+$ cells in 1:1 IL11/LOXL3 tumours, and occasional $IL11^+$ cells could still be detected in 1:18 IL11/LOXL3 tumours (Extended Data Fig. 9). Additionally, the resulting clonal frequencies were consistent with predictions of our mathematical model (Supplementary Information). Most probably, elimination of IL11 sub-clone restored microenvironmental barriers, thereby prohibiting the maintenance of a large tumour. These findings provide experimental support for the idea that a clone responsible for driving tumour outgrowth can be outcompeted by a clone with faster proliferation, leading to tumour collapse[24,25].

Discussion

Widespread tumour heterogeneity challenges the common assumption that tumour growth and malignant phenotypes are driven by dominant clones that have the highest cell-autonomous fitness advantage (Fig. 4g). Previous studies in *Drosophila* and mouse models demonstrated that tumour growth can be supported by a small population of cells via direct non-cell-autonomous stimulation[20,26,27]. Furthermore, the cross-talk between sub-populations of tumour cells has been implied in metastasis[28]. Our results suggest that tumours can be driven by a sub-population of cells that does not have higher fitness, but instead stimulate growth of all tumour cells non-cell-autonomously by inducing tumour-promoting microenvironmental changes (Fig. 4h, middle). Conversely, non-cell-autonomous clonal expansion does not necessarily translate into increased tumour growth rates (Fig. 4h, left). The non-cell-autonomous driver sub-clone can be outcompeted by a sub-clone with higher proliferative output, thus collapsing the tumour (Fig. 4h, right). Notably, in our experiments IL11-expressing cells were initially intermingled with the competitors. Under the scenario of stochastic activation of expression, benefits of secretion of non-cell-autonomously acting factors might be skewed to the producer clone due to spatial considerations. Therefore, although extensive intermingling of evolutionarily diverged sub-populations has been reported for primary tumours[29], it will be important to evaluate the effects of tumour topology in future studies.

Our results provide direct experimental evidence that clonal interference limits clonal expansions in tumours. Our modelling predicts that non-cell-autonomous driving of tumour growth can maintain clonal diversity over clinically relevant timeframes. In turn, clonal diversity can lead to clinically important phenotypic properties as suggested by the emergence of metastatic dissemination due to interactions between IL11- and FIGF-expressing sub-populations. Non-cell-autonomous driving of tumour growth and inter-clonal interactions suggest that experimental analysis and clinical diagnostics focusing only on the most abundant sub-population of tumour cells might be misleading.

Online Content Methods, along with any additional Extended Data display items and Source Data, are available in the online version of the paper; references unique to these sections appear only in the online paper.

Received 27 November 2013; accepted 3 June 2014.
Published online 30 July 2014.

1. Greaves, M. & Maley, C. C. Clonal evolution in cancer. *Nature* **481,** 306–313 (2012).
2. Nowell, P. C. The clonal evolution of tumor cell populations. *Science* **194,** 23–28 (1976).
3. Fearon, E. R. & Vogelstein, B. A genetic model for colorectal tumorigenesis. *Cell* **61,** 759–767 (1990).
4. Gerlinger, M. *et al.* Intratumor heterogeneity and branched evolution revealed by multiregion sequencing. *N. Engl. J. Med.* **366,** 883–892 (2012).
5. Landau, D. A. *et al.* Evolution and impact of subclonal mutations in chronic lymphocytic leukemia. *Cell* **152,** 714–726 (2013).
6. Ding, L. *et al.* Clonal evolution in relapsed acute myeloid leukaemia revealed by whole-genome sequencing. *Nature* **481,** 506–510 (2012).
7. Burrell, R. A., McGranahan, N., Bartek, J. & Swanton, C. The causes and consequences of genetic heterogeneity in cancer evolution. *Nature* **501,** 338–345 (2013).
8. Anderson, K. *et al.* Genetic variegation of clonal architecture and propagating cells in leukaemia. *Nature* **469,** 356–361 (2011).
9. Marusyk, A. & Polyak, K. Tumor heterogeneity: causes and consequences. *Biochim. Biophys. Acta* **1805,** 105–117 (2010).
10. Merlo, L. M., Pepper, J. W., Reid, B. J. & Maley, C. C. Cancer as an evolutionary and ecological process. *Nature Rev. Cancer* **6,** 924–935 (2006).
11. Weinberg, R. A. *The Biology of Cancer* (Garland Science, 2007).
12. Bissell, M. J. & Hines, W. C. Why don't we get more cancer? A proposed role of the microenvironment in restraining cancer progression. *Nature Med.* **17,** 320–329 (2011).
13. Gatenby, R. A. & Gillies, R. J. A microenvironmental model of carcinogenesis. *Nature Rev. Cancer* **8,** 56–61 (2008).
14. DeGregori, J. Challenging the axiom: does the occurrence of oncogenic mutations truly limit cancer development with age? *Oncogene* **32,** 1869–1875 (2013).
15. Kreso, A. *et al.* Variable clonal repopulation dynamics influence chemotherapy response in colorectal cancer. *Science* **339,** 543–548 (2013).
16. Gerrish, P. J. & Lenski, R. E. The fate of competing beneficial mutations in an asexual population. *Genetica* **102–103,** 127–144 (1998).
17. Putoczki, T. & Ernst, M. More than a sidekick: the IL-6 family cytokine IL-11 links inflammation to cancer. *J. Leukoc. Biol.* **88,** 1109–1117 (2010).
18. Ernst, M. *et al.* STAT3 and STAT1 mediate IL-11-dependent and inflammation-associated gastric tumorigenesis in gp130 receptor mutant mice. *J. Clin. Invest.* **118,** 1727–1738 (2008).
19. Putoczki, T. L. *et al.* Interleukin-11 is the dominant IL-6 family cytokine during gastrointestinal tumorigenesis and can be targeted therapeutically. *Cancer Cell* **24,** 257–271 (2013).
20. Inda, M. M. *et al.* Tumor heterogeneity is an active process maintained by a mutant EGFR-induced cytokine circuit in glioblastoma. *Genes Dev.* **24,** 1731–1745 (2010).
21. Bissell, M. J. & Radisky, D. Putting tumours in context. *Nature Rev. Cancer* **1,** 46–54 (2001).
22. Folkman, J. Angiogenesis in cancer, vascular, rheumatoid and other disease. *Nature Med.* **1,** 27–31 (1995).
23. Levayer, R. & Moreno, E. Mechanisms of cell competition: themes and variations. *J. Cell Biol.* **200,** 689–698 (2013).
24. Maley, C. C., Reid, B. J. & Forrest, S. Cancer prevention strategies that address the evolutionary dynamics of neoplastic cells: simulating benign cell boosters and selection for chemosensitivity. *Cancer Epidemiol. Biomarkers Prev.* **13,** 1375–1384 (2004).
25. Nagy, J. D. Competition and natural selection in a mathematical model of cancer. *Bull. Math. Biol.* **66,** 663–687 (2004).
26. Wu, M., Pastor-Pareja, J. C. & Xu, T. Interaction between Ras^{V12} and scribbled clones induces tumour growth and invasion. *Nature* **463,** 545–548 (2010).
27. Cleary, A. S., Leonard, T. L., Gestl, S. A. & Gunther, E. J. Tumour cell heterogeneity maintained by cooperating subclones in Wnt-driven mammary cancers. *Nature* **508,** 113–117 (2014).
28. Calbo, J. *et al.* A functional role for tumor cell heterogeneity in a mouse model of small cell lung cancer. *Cancer Cell* **19,** 244–256 (2011).
29. Navin, N. E. & Hicks, J. Tracing the tumor lineage. *Mol. Oncol.* **4,** 267–283 (2010).

Supplementary Information is available in the online version of the paper.

Acknowledgements We thank J. DeGregori, A. Goldman, A. Rozhok, M. Gonen and members of the Polyak and Michor laboratories for their critical reading of this manuscript and discussions. We thank L. Cameron in the DFCI Confocal Microscopy for her technical support. This work was supported by the Dana-Farber Cancer Institute Physical Sciences-Oncology Center (U54CA143798 to F.M.), CDRMP Breast Cancer Research Program W81XWH-09-1-0561 (A.M.), Cellex Foundation (V.A.), Deutsche Akademie der Naturforscher Leopoldina LPDS 2012-12 (P.M.A.) and the Breast Cancer Research Foundation (K.P.).

Author Contributions A.M. developed the experimental model, performed xenograft experiments and data analyses. D.P.T. performed immunohistochemical analyses and quantifications, and assisted with animal experiments. P.M.A. performed mathematical modelling and data analyses. V.A. assisted with image acquisition and analyses. K.P. supervised with help from F.M. All authors helped to design the study and write the manuscript.

Author Information Reprints and permissions information is available at www.nature.com/reprints. The authors declare no competing financial interests. Readers are welcome to comment on the online version of the paper. Correspondence and requests for materials should be addressed to K.P. (kornelia_polyak@dfci.harvard.edu).

METHODS

Cell lines. Breast cancer cell lines were obtained from the following sources: MDA-MB-468, MDA-MB-453, and HCC1954 from ATCC; MCF10DCIS.com from Dr. F. Miller (Karmanos Cancer Institute, Detroit, MI), SUM149PT from Dr. S. Ethier, University of Michigan, Ann Arbor, MI), and 21NT from Dr. A. Pardee (Dana-Farber Cancer Institute, Boston, MA). Cells were cultured in media recommended by the provider, their identity confirmed by short tandem repeats (STR) analysis, and regularly tested for mycoplasma.

Generation of MDA-MB-468 derivate lines ('sub-clones'). Entry cDNA ORFs in pDONOR223 or pENTR221 were obtained from human ORFeome collection v5.1 or Life Technologies, respectively. Lentiviral expression constructs were generated by Gateway swap into pLenti6.3/V5-Dest vector (Life Technologies) or pHAGE-EF (used for IL11 swap only, vector obtained from S. Elledge laboratory, Harvard Medical School) destination vectors and sequence verified. Assembling viral particles and transductions were performed following Life Technology protocols. Parental MDA-MB-468 cell lines were transduced with mCherry/Luciferase lentiviral construct (obtained from C. Mitsiades laboratory, DFCI) before derivation of specific sub-clones. Each derivative line was generated from a pool of 1×10^5 to 2×10^5 transduced cells. Lentiviral-mediated expression was verified by immunoblotting against V5 tag *in vitro* and further confirmed by immunohistochemistry *in vivo*. The GFP sub-clone was derived by lentiviral transduction of pLVX-AcGFP (Life Technologies).

qPCR analysis of clonal composition. The frequency of individual clones within tumours was determined by analysing the change in qPCR signal from the initial mixture, which was precisely defined through mixing of clones based on cell counts, and the terminal tumour. qPCR was performed using Life Cycler 4800 (Roche) using SYBR green method with reaction mixtures purchased from Kapa Biosystems. Signals from individual clones were determined using a primer anchored in lentiviral backbone (anchor) and a primer specific for the clone-defining factor. As an internal reference we used primers specific for the peri-centromeric region of chromosome 12, which does not display copy number alterations in the MDA-MB-468 cell line. Primer sequences are listed below. The primers employed in the quantitation displayed linear amplification with >95% amplification efficiency. Change of frequency relative to the initial mixture was determined from Ct values for clone specific and internal reference qPCR signal based on ddCt method. Clonal proportions in polyclonal tumours were normalized based on total frequency of 1. For calculation of fold expansion, we used the clonality data to infer number of cells, following inferences between tumour mass and cellularity as described in the Supplementary Information.

Target sequence of primers. pLenti6.3/V5-Dest expressed: anchor TCCAGTGT GGTGGAATTCTG; IL11 CGTCAGCTGGGAATTTGTC; SPP1 CATTCTGTG GGGCTAGGAGA; VEGFC GAGCACTTGCCACTGGTGTA; IHH GGTCTGA TGTGGTGATGTCC; HGF CTTTTCCTTTGTCCCTCTGC; CCL5 CTGCTCC TCCAGATCTTTGC; VEGFB CCATGAGCTCCACAGTCAAG; FIGF CTCCA CAGCTTCCAGTCCTC; CXCL12 ATCTGAAGGGCACAGTTTGG; VCAN GC GGAGAAATTCACTGGTGT; SHH CCACATTGGGGATAAACTGC; VEGFA GATTCTGCCCTCCTCCTTCT; CXCL14 TTTGGCTTCATTTCCAGCTT; LOXL1 ACTATGAGCCCGAGTTGAGC; LOXL3 GTCTTCGATGTAGGCGGTCT; AN GPTL4 GCGCCAGGACATTCATCT; IL6 GCGGCTACATCTTTGGAATC; LA CZ CGGGCCTCTTCGCTATTAC; pLVX-AcGFP expressed; GFP F TCCTGGG CAATAAGATGGAG; GFP R TGGGGGTATTCTGCTGGTAG; pHAGE-EF-DEST expressed: anchor TGGGACGTCGTATGGGTATT; IL11 GGCTGCACCTGAC ACTTGAC; human-specific centromeric reference locus; F TTTGGGGCCTTAA CACTTT; R AAGCAACCAGAAGCCTTTCA.

Xenograft experiments and doxorubicin treatment. All animal procedures were approved by the DFCI ACUC (DFCI protocol#11-023) and followed NIH guidelines. Tumours were induced by bilateral orthotopic injection into 4–5-weeks old female *Foxn1*^{nu} mice of 1×10^6 cells resuspended in 50% Matrigel (BD Biosciences) per transplant. Animals without successful tumour grafting were excluded from the analysis. Tumour volumes were monitored by bi-weekly measurements of tumour diameters with electronic calipers. For doxorubicin treatment, animals were injected at days 15 and 22 post-transplantation with 5 mg per kg doxorubicin or PBS control. As tumour sizes distribution of control and treatment groups before treatment was similar, no randomization was performed. No blinding was performed during the tumour measurements in live animals.

Immunoblot analysis. A total of 2×10^6 cells per sample were lysed in 100 µl of RIPA buffer. 10 µl of lysate was loaded per well of 4–12% Bis-Tris NuPage Midi gel (Life Technologies). Proteins were transferred to Immobilon PVDF membrane (EMD Millipore, Billerica, USA). Membranes were blocked for 30 min in StartingBlock blocking buffer (Thermo Scientific, Waltham, MA), then incubated overnight at 4°C with primary antibodies diluted 1:1,000 in PBST in presence of 2.5% BSA. After 3× 5 min washes, membranes were incubated with secondary antibodies at 1:20,000 dilution, washed 2× 5 min followed by a 20 min wash. The membranes were developed with Immobilon substrate (EMD Millipore, Billerica, USA). The following antibodies were used: β-actin (Sigma, # A2228), IL11Rα (R&D systems #MAB1977), HRP conjugated anti-mouse and anti-rabbit (Thermo Scientific).

shRNA experiments. shRNA constructs in pLKO lentiviral vectors were obtained from the Broad Institute RNAi consortium. shRNA with the following targeting sequences were used: IL11Ra shRNA#4 CGGCAGATTCCACCTATAATT; IL11Rα shRNA#5 TGGGACCATACCAAAGGAGAT; IL11Rα shRNA#7 TGGAGCCA GTACCGGATTAAT; IL11Rα shRNA#8 TGGCGTCTTTGGGAATCCTTT; IL11Rα shRNA#9 ACTGATGAGGGCACCTACATC.

IL11 ELISA. Cells were plated at 1×10^5cells per well in a 6-well plate and left overnight at 37°C with 5% CO_2. The next morning, the media was replaced and the cells returned to the incubator. After 5 h of incubation, the cells and the media were collected on ice in order to determine the concentrations of intracellular and secreted IL11, respectively. The harvested cells were counted, resuspended in PBS and lysed by rapid freeze thaw cycles. The media and cell lysates were used for human-IL11 ELISA (RayBiotech; ELH-IL11-001) according to the manufacturer's instructions. The values were adjusted for cell numbers as well as final volume to get an estimate of relative concentrations of IL11 in the two vector derivates.

Histological, immunohistochemical and multicolor immunofluorescence analyses. For histological analyses, 5-µm sections of formalin fixed paraffin embedded (FFPE) xenografts were stained with haematoxylin and eosin using standard protocols. For analyses of collagen content, the tumour sections were stained with Masson's trichrome stain kit (American Mastertech) following the manufacturer's instructions. Immunohistochemical analyses of bromodeoxyuridine (BrdU, Roche cat#11170376001, clone BMC9318, mouse monoclonal IgG_1, 1:100), Ki-67 (Dako M724001, clone MIB-1, mouse monoclonal IgG_1, 1:100), CD31 (Neomarkers RB10333, rabbit polyclonal, 1:50) and smooth muscle actin (SMA, Dako M085101, clone 1A4, mouse monoclonal IgG2a, 1:250) were performed using 5-µm sections of FFPE xenografts. The tissues were deparaffinized and rehydrated. After heat-induced antigen retrieval in citrate buffer (pH 6 for BrdU and Ki-67) or Dako target retrieval solution (S2367, pH 9 for CD31 and SMA), the samples were blocked with 3% hydrogen peroxide in methanol followed by goat serum and stained with the primary for 1 h at room temperature. The samples were then incubated with anti-mouse or anti-rabbit IgG biotinylated antibody (1:100 dilution) for 30 min at room temperature followed by the ABC peroxidase system (Vectastain, ABC System Vector Laboratories). DAB (3,3′-diaminodbenzidine) was used as the colorimetric substrate. The samples were washed twice with PBS-Tween 0.05% between incubations. Then the slides were counterstained with Harris haematoxylin or 1% methyl green. Scoring for the expression of each marker was done as follows: the percentage of $Ki67^+$ and $BrdU^+$ cells were estimated by counting an average of 1,500–2,000 cells per sample using ImageJ 1.45 s software from 4–6 randomly selected regions of the xenografts. Vessel density was scored by counting the number of $CD31^+$ vessels per 20× field for 4–6 randomly selected fields in the tumour and the average was calculated. Blinding was used during key quantification analyses.

Multicolour immunofluorescence for cleaved caspase 3 (Cell Signaling cat#9661, rabbit monoclonal IgG, 1:50) and/or V5 (Invitrogen R960-25, mouse monoclonal IgG_{2a}, 1:100 was performed similarly as above. After heat-induced antigen retrieval at pH 6, the samples were blocked with goat serum and stained with the primary overnight at 4°C followed by incubation with goat anti-rabbit IgG Alexa 488-conjugated (Life Technologies, 1:100 dilution, for detection of cleaved caspase 3) and goat anti-mouse IgG_{2a} Alexa 555-conjugate (Life Technologies, 1:100 dilution, for detection of V5) for 45 min at room temperature. The samples were protected for long-term storage with VECTASHIELD HardSet Mounting Medium with DAPI (Vector laboratories, cat #H-1500). Before image analysis, the samples were stored at −20°C for at least 48 h. Different immunofluorescence images from multiple areas of each sample were acquired with a Nikon Ti microscope attached to a Yokogawa spinning-disk confocal unit using a 60× plain apo objective, and OrcaER camera controlled by Andor iQ software. The montage images were created using the stitching plugin[30] in (Fiji Is Just) ImageJ 1.48f software.

Terminal deoxynucleotidyl transferase dUTP nick end labelling (TUNEL) assay. FFPE sections of the xenografts were deparaffinized and rehydrated. Sections were then treated with 60 µg ml^{-1} proteinase K (20 mg ml^{-1}, Invitrogen, DNase- and RNase-free) in PBS for 15 min at room temperature. Protease digestion was stopped by consecutive washes in PBS and TdT buffer (Thermo Scientific). The sections were blocked with 3% hydrogen peroxide in methanol to inhibit endogenous peroxidase activity. TUNEL assays were performed at 37°C for 1 h in TdT buffer, 150 mM NaCl, 2 µM biotin 16-dUTP (Roche) and 80 U per ml TdT (Thermo Scientific ; EP0162). Following washing in PBS, labelled cells were visualized with the ABC peroxidase System (Vectastain, ABC System Vector Laboratories) using DAB (3,3′-diaminodbenzidine) as the colorimetric substrate. The slides were counterstained with Harris haematoxylin. The percentage of $TUNEL^+$ cells were estimated

by counting an average of 600–1000 cells per sample using ImageJ 1.45 s software from 4–6 randomly selected regions of the tumours.

Statistical analysis. Sample size was determined based on pilot experiments followed by larger-scale studies to obtain significant differences (including the animal experiments). Estimation of variation within experimental group, normality test and statistical analyses indicated in figure legends were performed with Prism software (Graph Pad), or with Wolfram Mathematica. Unless otherwise specified, *P* values refer to the results of the two-tailed *t*-test.

30. Preibisch, S., Saalfeld, S. & Tomancak, P. Globally optimal stitching of tiled 3D microscopic image acquisitions. *Bioinformatics* **25,** 1463–1465 (2009).

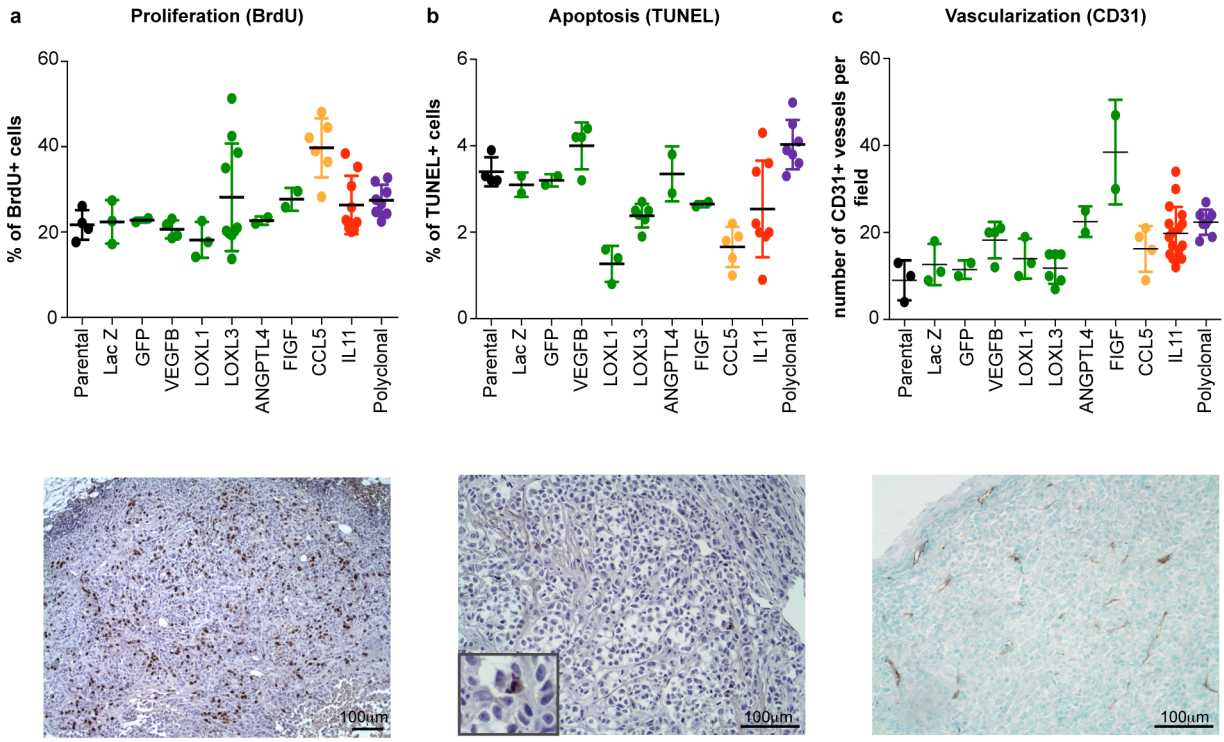

Extended Data Figure 1 | Proliferation, apoptosis and vascularization in selected groups. **a**–**c**, Quantification and representative pictures of immunohistochemical analysis for markers of proliferation (**a**), apoptosis (**b**), and vascularization (**c**). Each dot represents an individual tumour, error bars indicate s.d.

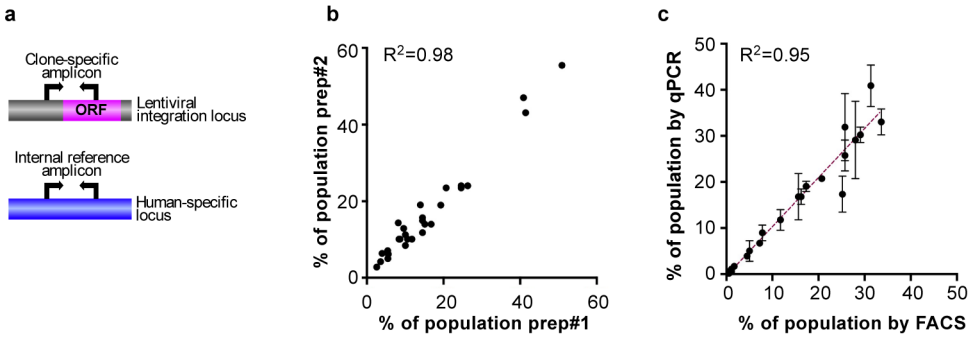

Extended Data Figure 2 | Estimations of clonal frequencies. **a**, Schematic outline of the quantification of clonal composition based on qPCR. Changes in clonal frequencies are determined based on changes in the ratios of clone-specific and a human-specific reference amplicon between initial mixtures and the resulting tumours. **b**, Reproducibility of clonality analysis between two different DNA preparations/qPCR from same tumour. **c**, Correlation between the results obtained using fluorescent-activated cell sorting (FACS) and qPCR based determination of clonal frequency after 6 weeks *in vitro* culture. Green fluorescent protein (GFP) labelled parental cells were mixed with individual sub-clones at initial ratios of 20:1. R^2 indicates goodness of fit of linear regression.

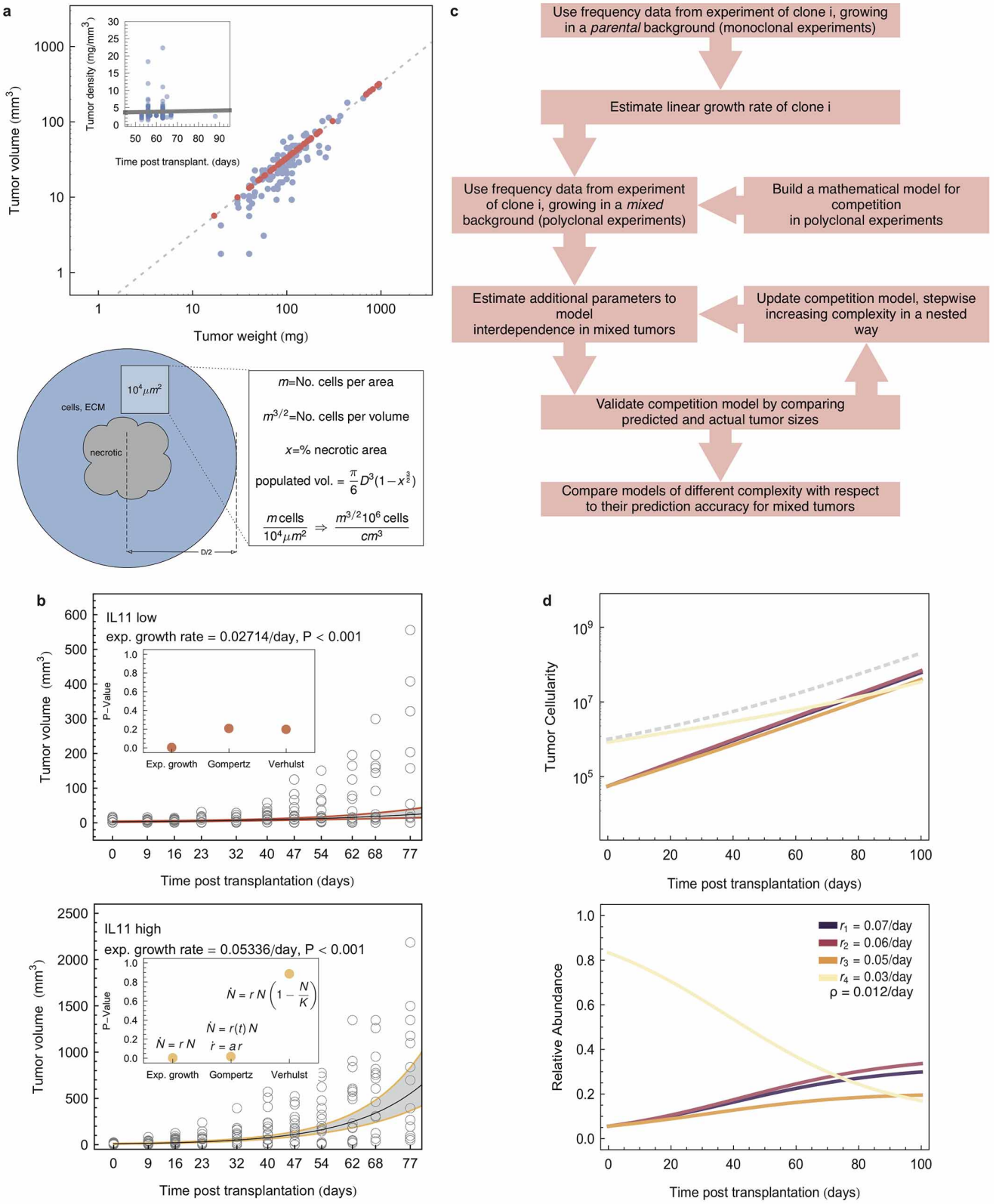

Extended Data Figure 3 | Mathematical model. **a**, Upper panel: estimation of tumour volume–density relation. The dashed line represents a linear regression with slope 0.33 ($P < 0.01$). Red dots are predictions for which one value of the pair was missing. Inset, tumour density over time from clone-vs-parental competition experiments (dots). Tumour density did not correlate with the time of sample collection (line, linear regression with slope 0.012, $P = 0.68$). Lower panel, schematic of estimation of cell numbers in tumour samples from two dimensional slices. **b**, Tumour volume over time from experiments (empty circles) and linear regression (exponential tumour growth law, black lines), with 0.95 confidence intervals (grey areas). Inset: comparison of P values using different growth laws. **c**, Flow chart of mathematical modelling approach. **d**, Upper panel, growth dynamics under non-cell-autonomous driving, according to mathematical model (model B, see Supplementary Information), driver effect of IL11 was set to a typical value of 0.012/day. Example of four individual sub-clones (for example, IL11, LOXL3, slow-growing CCL5, LacZ), total tumour size indicated by dashed line; lower panel, frequency dynamics for the same set.

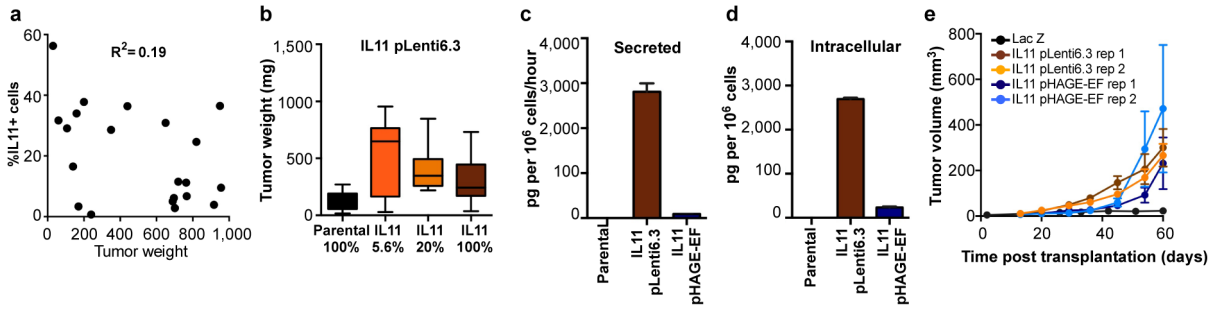

Extended Data Figure 4 | Reproducibility and frequency-independence of tumour-growth promoting effects of IL11. **a**, Relation between tumour weight and fraction of IL11 sub-clone cells upon tumour sample collection. **b**, Final weights of tumours initiated from the indicated mixtures of IL11 expressing and parental cells using pLenti6.3 backbone; $n = 21$ for the 5.6% IL11, $n = 10$ for the other groups. **c**, **d**, Secreted (pg per 10^6 cells per hour) (**c**) and intracellular (pg per 10^6 cells) (**d**) levels of IL11 protein determined by ELISA in parental cells and in the IL11-expressing clones derived using the indicated lentiviral constructs. **e**, Growth kinetics of tumours initiated by transplantation of mixtures containing IL11-expressing cells from the indicated backbones competing with the parental cells.

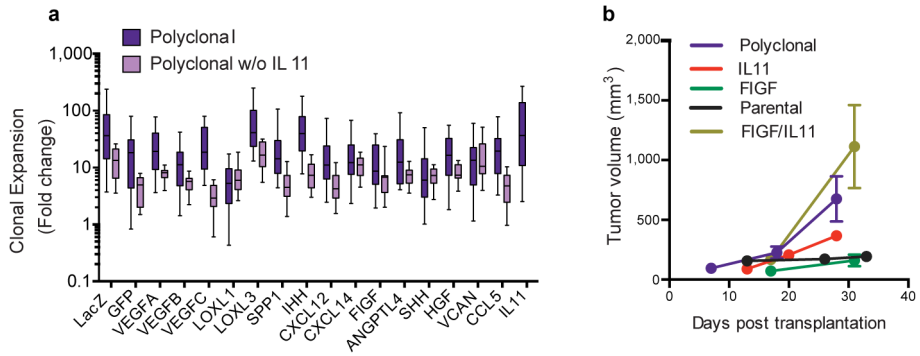

Extended Data Figure 5 | IL11 in clonal cooperation. **a**, Expansion (fold-change over initial number of cells) of indicated sub-clones in the polyclonal tumours initiated with/without IL11 sub-clone, $n = 10$ per group. **b**, Growth curves of the tumours initiated by transplantation of the indicated groups, IL11 + FIGF indicates tumours initiated by 1:1 mixtures of IL11 and FIGF sub-clones.

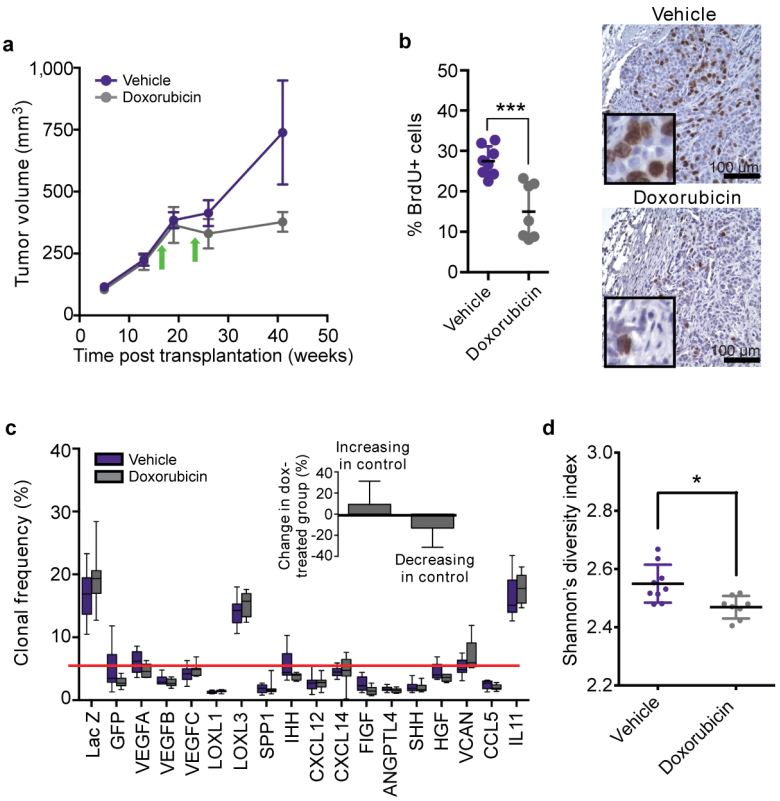

Extended Data Figure 6 | The effects of doxorubicin on tumour growth and clonal composition. **a–c,** Tumour growth (**a**), assessment of cell proliferation by BrdU staining (**b**) and clonal composition (**c**) of tumours initiated by polyclonal mixtures followed by treatment of the animals bearing established tumours with vehicle control or doxorubicin. Arrows mark intraperitoneal injections of doxorubicin (5 mg per kg) or vehicle. The inset in **c** quantifies changes in frequency of clones expanding and shrinking compared to the initial frequencies. Interaction factor for two-way ANOVA between control and doxorubicin groups is statistically significant ($P = 0.0059$). **d**, Shannon index for clonal diversity of vehicle and doxorubicin treated tumours, $*P < 0.05$ in two-sample Kolmogorov–Smirnov test.

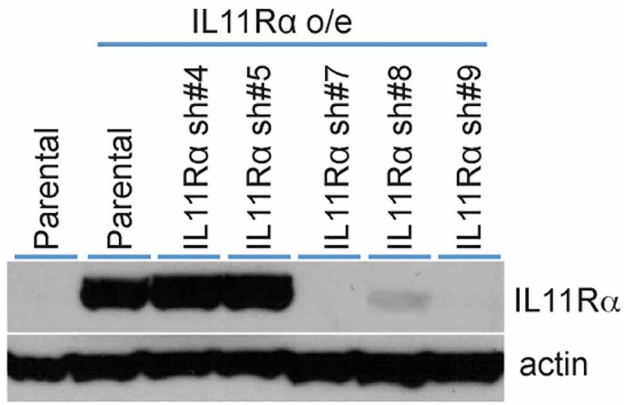

Extended Data Figure 7 | Validation of IL11Rα shRNA. As the commercially available IL11Rα antibodies are not sufficiently sensitive to detect endogenous IL11Rα protein in the MDA-MB-468 cells, we tested the ability of shRNA to downregulate the expression of exogenously expressed IL11Rα. Cells overexpressing IL11Rα were stably transduced with IL11Rα-targeting shRNAs and the expression of IL11Rα and β-actin (loading control) were analysed by immunoblotting.

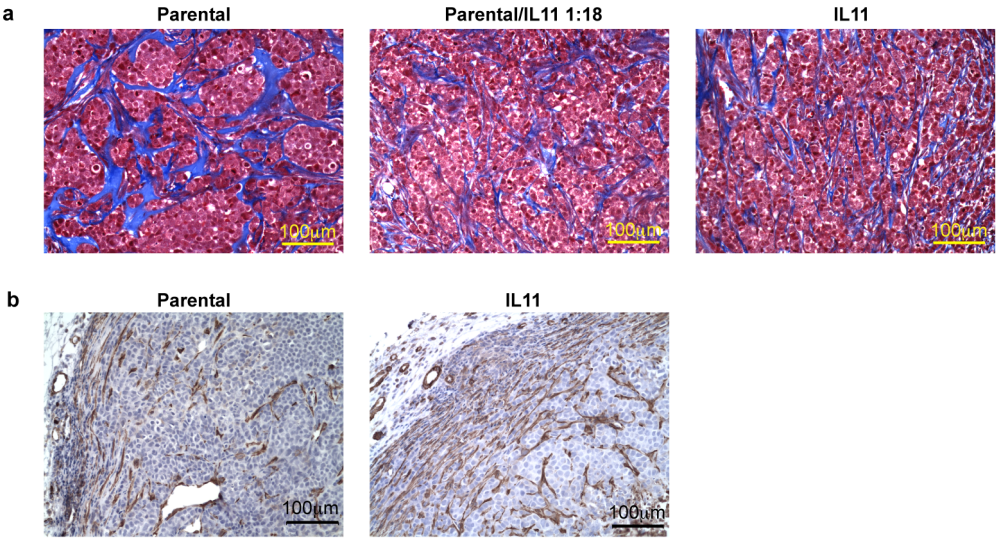

Extended Data Figure 8 | The effects of IL11 on the tumour microenvironment. **a**, Collagen organization in parental and IL11 expressing tumours. Representative images of collagen structure (blue) in the indicated tumours as determined by tri-chrome staining. **b**, Smooth muscle actin positive (SMA) stromal cells in control and IL11 expressing tumours. Representative images of immunohistochemical staining for SMA.

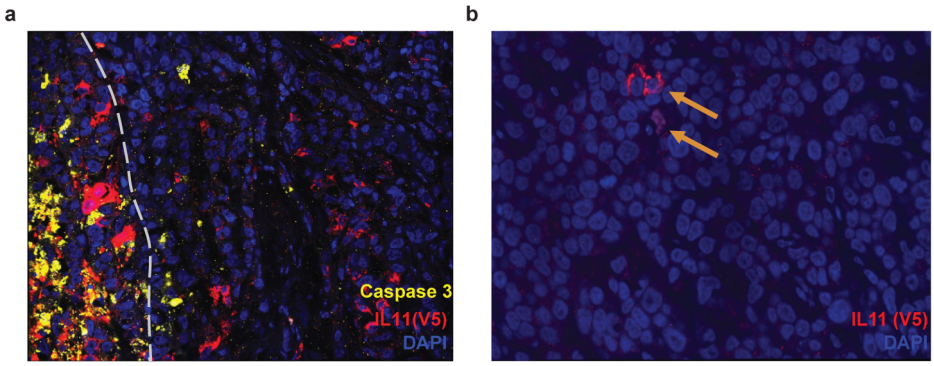

Extended Data Figure 9 | IL11 cells are not specifically eliminated in IL11/LOXL3 tumours. **a**, Immunofluorescence analysis of apoptosis in 1:1 IL11/LOXL3 tumours. Apoptotic marker cleaved caspase 3 (yellow) indicates lack of increase in apoptosis in IL11 (red, $V5^{+}$) cells bordering LOXL3 ($V5^{-}$, as LOXL3 cDNA has a stop codon before the tag). Grey dashed line demarcates the border of the necrotic area, where most of cell death occurs. **b**, Occasional $IL11^{+}$ cells (indicated by arrows) could still be detected in the remnants of 1:18 IL11/LOXL3 tumours.

Extended Data Table 1 | List of factors employed in sub-clonal derivations

Official gene symbol	Official gene name	Rationale for picking
LACZ	beta-D-galactosidase	Control
GFP	green fluorescent protein	Control
VEGFA	vascular endothelial growth factor A	Angiogenesis
VEGFB	vascular endothelial growth factor B	Lymphangiogenesis, metastasis
VEGFC	vascular endothelial growth factor C	Angiogenesis, ,ymphangiogenesis, and metastasis
LOXL1	lysyl oxidase-like 1	Invasion and metastasis
LOXL3	lysyl oxidase-like 3	Invasion and metastasis
SPP1	secreted phosphoprotein 1	Promotion of tumor growth through recruitment of bone marrow-derived cells
IHH	indian hedgehog	Activation of stroma
FIGF	c-fos induced growth factor	Lymphangiogenesis, metastasis
CXCL12	chemokine (C-X-C motif) ligand 12	Leukocyte infiltration, proliferation, metastasis
CXCL14	chemokine (C-X-C motif) ligand 14	Increased motility and invasiveness
SHH	sonic hedgehog	Promotion of tumor growth
VCAN	versican	Invasion, metastasis and growth
HGF	hepatocyte growth factor	Migration, adhesion and angiogenesis
CCL5	chemokine (C-C motif) ligand 5	Recruitment of monocytes
IL11	interleukin 11	Bone metastasis
ANGPTL4	angiopoietin-like 4	Angiogenesis and metastasis
IL6*	interleukin 6	Survival, proliferation

* An IL6 expressing sub-clone was generated and tested in the pilot experiments but was excluded due to high systemic toxicity.